Int J Adv Manuf Technol (2015) 76:1593–1606
DOI 10.1007/s00170-014-6346-x

ORIGINAL ARTICLE

Effect of arc mode in cold metal transfer process on porosity of additively manufactured Al-6.3%Cu alloy

Baoqiang Cong · Jialuo Ding · Stewart Williams

Received: 5 March 2014 / Accepted: 3 September 2014 / Published online: 23 September 2014

Abstract In this study, the effect of arc mode in cold metal transfer (CMT) process on the porosity characteristic of additively manufactured Al-6.3%Cu alloy has been systematically investigated. The variants include conventional CMT, CMT pulse (CMT-P), CMT advanced (CMT-ADV) and CMT pulse advanced (CMT-PADV) and experiments were performed on both single layer deposits and multilayer deposits. The mechanism of porosity generation using the CMT arc mode variants is discussed. It was found that deposit porosity is significantly influenced by the arc mode type of CMT process. Conventional CMT is not suitable for the additive manufacturing process because it produces a large amount of gas pores, even in single layer deposit. CMT-PADV proved to be the most suitable process for depositing aluminium alloy due to its excellent performance in controlling porosity. With correct parameter, setting the gas pores can be eliminated. It was found that the key factors that enable the CMT-PADV process to control the porosity efficiently are the low heat input, a fine equiaxed grain structure and effective oxide cleaning of the wire.

Keywords Aluminium alloy · Additive manufacture · Cold metal transfer · Arc mode · Porosity

B. Cong (✉)
School of Mechanical Engineering and Automation, Beihang University, Beijing 100191, People's Republic of China
e-mail: congbq@buaa.edu.cn

J. Ding · S. Williams
Welding Engineering and Laser Processing Centre, Cranfield University, Cranfield MK43 0AL, UK

1 Introduction

High strength aluminium alloys have gathered wide acceptance in aeronautic and aerospace applications due to their excellent strength, fracture properties and good corrosion resistance. The conventional method of manufacturing aluminium alloy components is using subtractive processes which machine the component out of a solid alloy block. Most of the aluminium alloy needs to be machined away which results in a long production time and high cost. In addition it cannot satisfy the requirement for sustainability of modern industry. Thus, more attention has been focused on the metal additive manufacturing (AM), which has proved to be an economic alternative method for fabricating metal components. Among different AM processes, wire plus arc additive manufacture (WAAM) is becoming more popular due to its high deposition rate, low production cost and the capability for fabricating large-scale components [1, 2].

In a previous research, several papers have reported on AM of aluminium alloys. Variable polarity gas tungsten arc welding was employed for fabricating components with Al-4043 and Al-5356 alloys [3–5], and selective laser melting has been used to deposit AlSi10Mg alloy [6, 7]. From this literature, it was identified that porosity is a major problem in making aluminium components using AM processes. This can severely restricts the mechanical performance of the components produced.

The cold metal transfer (CMT) process is a relatively new technique which is characterised by its low heat input, low spatter and high deposition rate. Welding of aluminium alloy thin plates and low dilution cladding of aluminium alloy has been studied using the CMT process

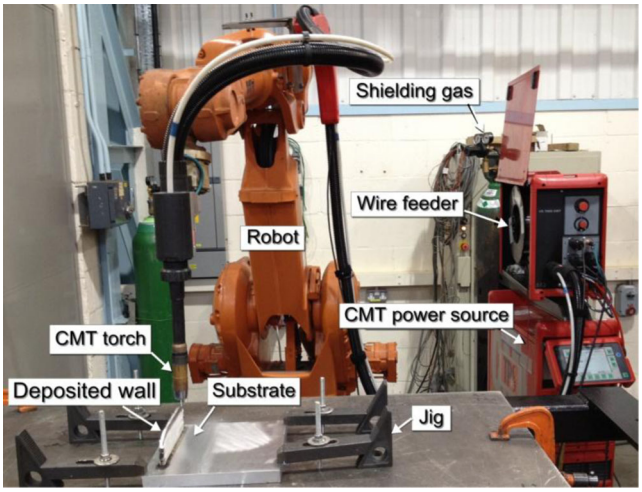

Fig. 1 CMT WAAM experimental system

[8–10]. It has been observed that this process exhibits greater control of droplet transfer and dilution. Recently CMT has been developed into different droplet transfer modes which are conventional CMT, CMT pulse (CMT-P), CMT advanced (CMT-ADV) and CMT pulse advanced (CMT-PADV). Due to the excellent characteristics in terms of low spatter and automatic adjustment of contact tip to work distance, the CMT process is a potential process to be used in the AM application of aluminium alloy. However, the porosity characteristic of using different arc mode in the CMT process on deposited aluminium alloy is unknown. In this paper, the porosity characteristic of additively manufactured Al-6.3 % Cu alloy was investigated. Different CMT arc modes were employed and their influence on the porosity was analysed. The mechanism of porosity generation for these different modes is discussed.

Table 1 Parameters for the single layer deposits

Conventional CMT
WFS=7.5 m/min, TS=0.5–1.0 m/min, HI=165.8–331.6 J/mm
CMT-P
WFS=7.5 m/min, TS=0.5–1.0 m/min, HI=183.4–366.8 J/mm
CMT-ADV
WFS=7.5 m/min, TS=0.4–0.8 m/min, HI=170.8–341.6 J/mm
CMT-PADV
WFS=7.5 m/min, TS=0.4–0.5 m/min, HI=135.4–169.3 J/mm

2 Experimental

The material used was 1.2 mm diameter AA2319 wire with a chemical composition of Cu 6.3, Mn 0.3, Zr

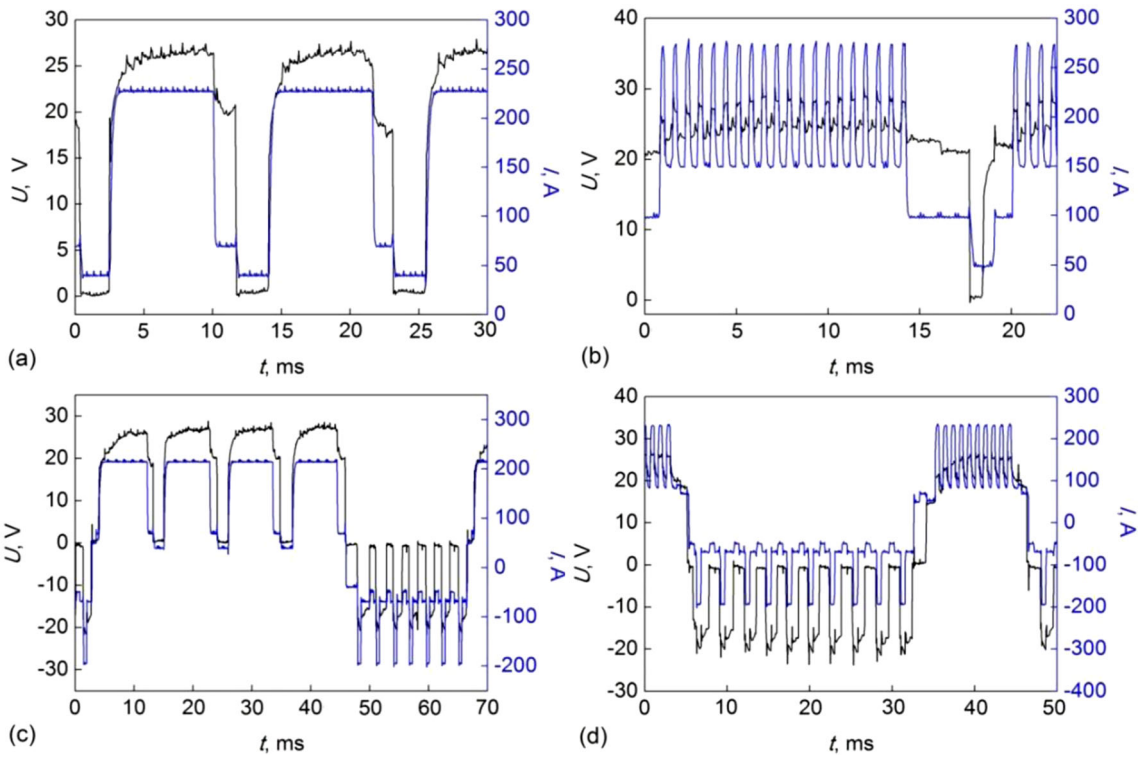

Fig. 2 Arc current and voltage waveforms of CMT (**a**), CMT-P (**b**), CMT-ADV (**c**) and CMT-PADV process (**d**; WFS=7.5 m/min)

Table 2 Parameters for multilayer wall additive manufacture

CMT-P
WFS=5–6 m/min, TS=0.8–1.0 m/min, layer number 14 or 20
HI=137.1–189.1 J/mm
CMT-ADV
WFS=6–7.5 m/min, TS=0.5–0.8 m/min, layer number 10
HI=135.7–273.4 J/mm
CMT-PADV
WFS=6–7.5 m/min, TS=0.4–0.6 m/min, layer number 10 or 14
HI=112.2–168.4 J/mm

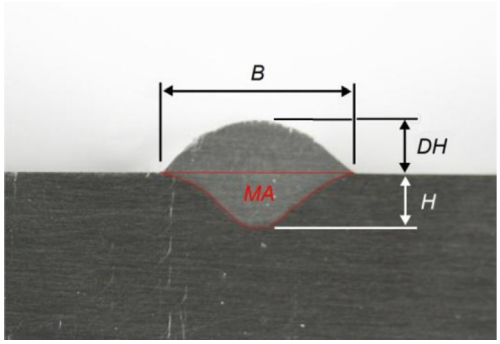

Fig. 3 Schematic diagram of single layer deposit geometry (*B* width of single layer deposit, *DH* height of single layer deposit, *H* substrate melting depth, *MA* melted area of single layer deposit)

0.175, Ti 0.15, V 0.1 and Al balance (all in wt.%) and the wire was used in its as-received condition. Substrates were wrought AA2219 (temper T851) 19 mm thick plates with a chemical composition of Cu 6.3, Mn 0.3, Si 0.2, Fe0.3, Zr 0.18 and Al balance (all in wt.%). All substrates were cleaned shortly before being used, by degreasing with acetone and linishing afterwards.

The WAAM system used in this study is shown in Fig. 1. A Fronius CMT Advanced 4000 R was employed as the power source. This system is designed to supply four droplet transfer modes, which are conventional CMT, CMT-P, CMT-ADV and CMT-PADV. An ABB robot IRB2400 was employed to provide accurate and repeatable movement. For all the trials, pure argon (99.99 %) was used as the shielding gas with a constant flow rate of 25 L/min. The contact tip to work distance (CTWD) was kept to 15 mm for all the trials.

Arc current and voltage of these four different arc modes were monitored by using the AMV4000 equipment. Figure 2 shows the actual arc current and voltage waveforms for these four modes with constant wire feed speed (WFS) of 7.5 m/min. In this study, all the experiments were carried out in an open atmosphere with torch shielding only. In the first experiments, single layer deposit samples 100 mm in length were

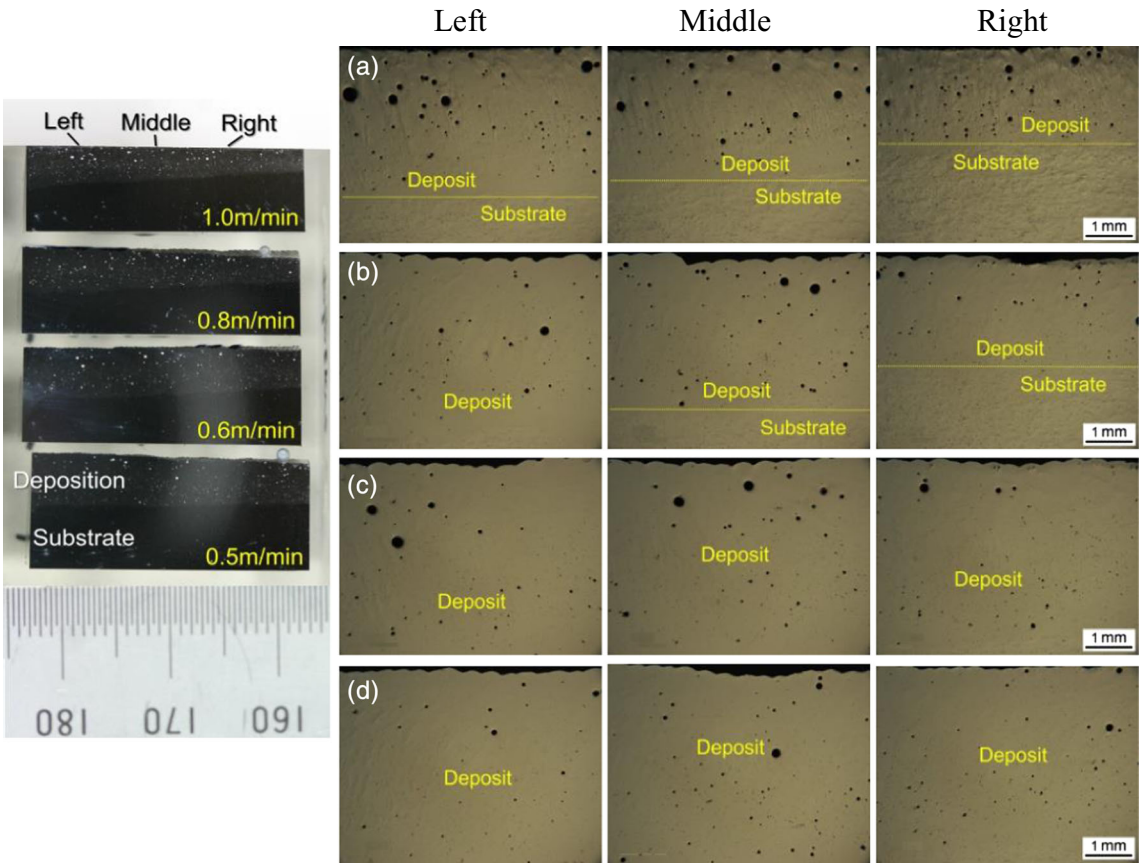

Fig. 4 Optical micrographs showing single layer deposit porosity with conventional CMT process: **a** TS=1.0 m/min, HI=165.8 J/mm, **b** TS=0.8 m/min, HI=207.3 J/mm, **c** TS=0.6 m/min, HI=276.3 J/mm and **d** TS=0.5 m/min, HI=331.6 J/mm

made using the four modes. Constant WFS and variable travel speed (TS) were utilised; details are given in Table 1. The heat input (HI) for different trials were calculated using the formula $HI=\eta\times(\sum U_i I_i)/TS$ [11], where U_i and I_i are arc voltage and current for each sample, respectively, and η is the arc thermal efficiency of CMT that is set to 0.8 [12, 13]. In the second experiments, multilayer additively manufactured wall samples of 150 mm in length were built using different WFS and TS settings. The setting details as well as the calculated heat input for each trial are shown in Table 2.

All samples were cut using an automatic machining (Discotom-60, Struers) along longitudinal and transverse directions including the substrate. They were polished using a standard metallographic procedure, which consisted of grinding followed by polishing and etching. Specimens were etched with the standard Kroll's reagent solution (6 mL HNO_3, 2 mL HF, 92 mL H_2O). Porosity and microstructure examinations were carried out using an optical microscope (OPTIPHOT, Nikon, Japan). Pore counts were performed on each single layer deposit sample over a 15-mm representative middle section in the longitudinal direction. The pore sizes were measured using Axio Vision SE64 software. The transverse geometry of the single layer deposit samples was characterized as shown in Fig. 3 and measured using Axio Vision SE64 software.

3 Results and discussions

3.1 Porosity of single layer deposits

AA2219 single layer deposit samples produced by the four different modes have excellent surface appearance with effective oxide cleaning. Figures 4, 5, 6 and 7 illustrate the distributions of gas pores using different modes with different parameter settings. Figure 8 shows the gas pore counts sorted by the diameters of the pores in each sample. It can be seen that the arc mode has a significant influence on the porosity. In all samples most of the gas pores were micro sized (10–50 μm). Compared to the other three modes, the conventional CMT

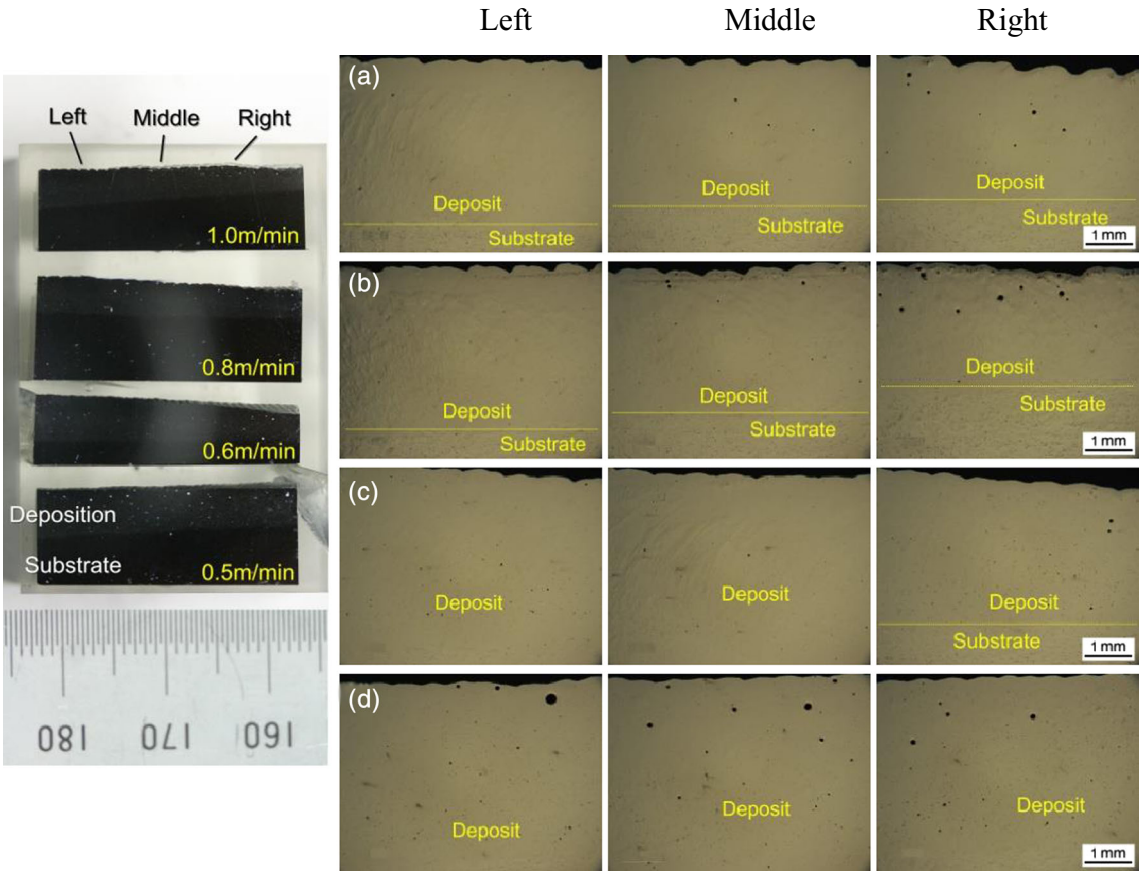

Fig. 5 Optical micrographs showing single layer deposit porosity with CMT-P process: **a** TS=1.0 m/min, HI=183.4 J/mm, **b** TS=0.8 m/min, HI=229.3 J/mm, **c** TS=0.6 m/min, HI=305.7 J/mm and **d** TS=0.5 m/min, HI=366.8 J/mm

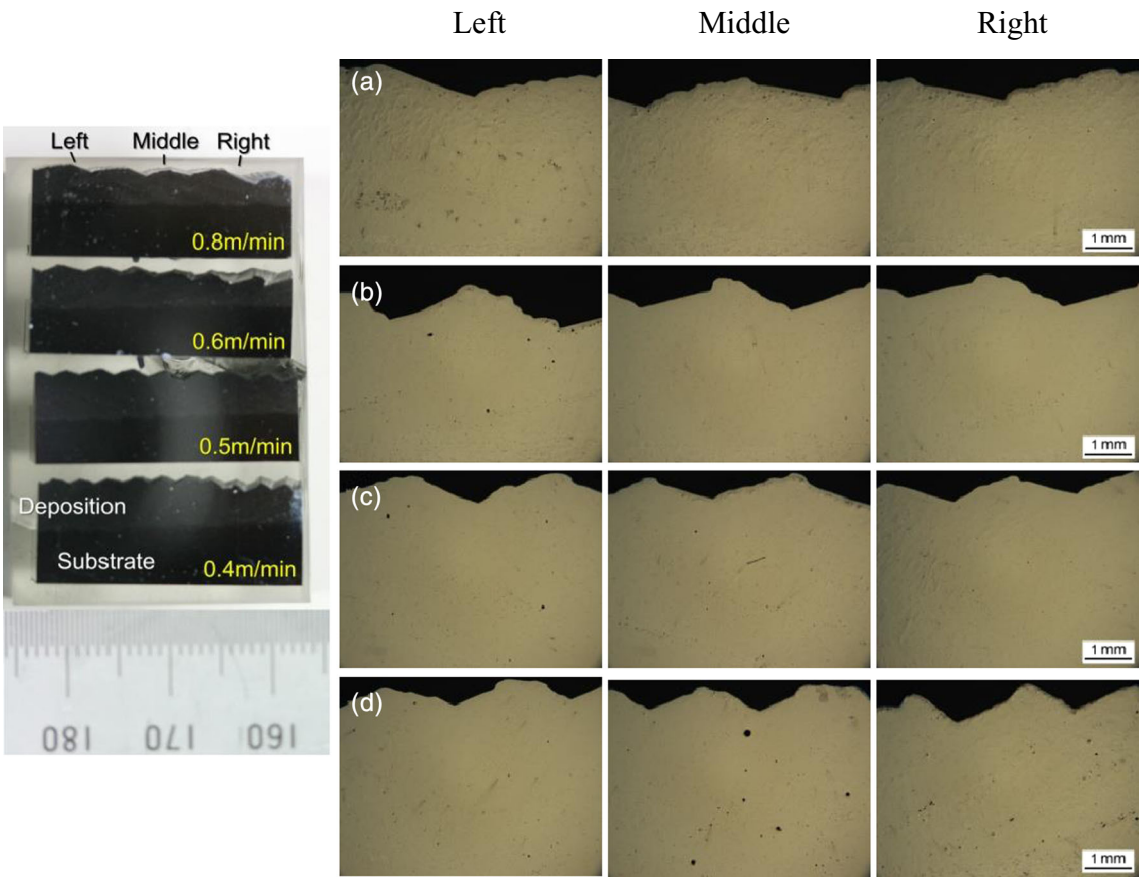

Fig. 6 Optical micrographs showing single layer deposit porosity with CMT-ADV process: **a** TS=0.8 m/min, HI=170.8 J/mm, **b** TS=0.6 m/min, HI=227.8 J/mm, **c** TS=0.5 m/min, HI=273.4 J/mm and **d** TS=0.4 m/min, HI=341.6 J/mm

process produced the largest number of gas pores and some gas pores were larger than 100 μm in diameter. The CMT-P process significantly reduced the number of gas pores and the size of gas pores. The CMT-ADV process further reduced the number and size of gas pores. There were virtually no gas pores which were larger than 50 μm in diameter. The CMT-PADV process nearly eliminated the gas pores in the single layer deposit samples.

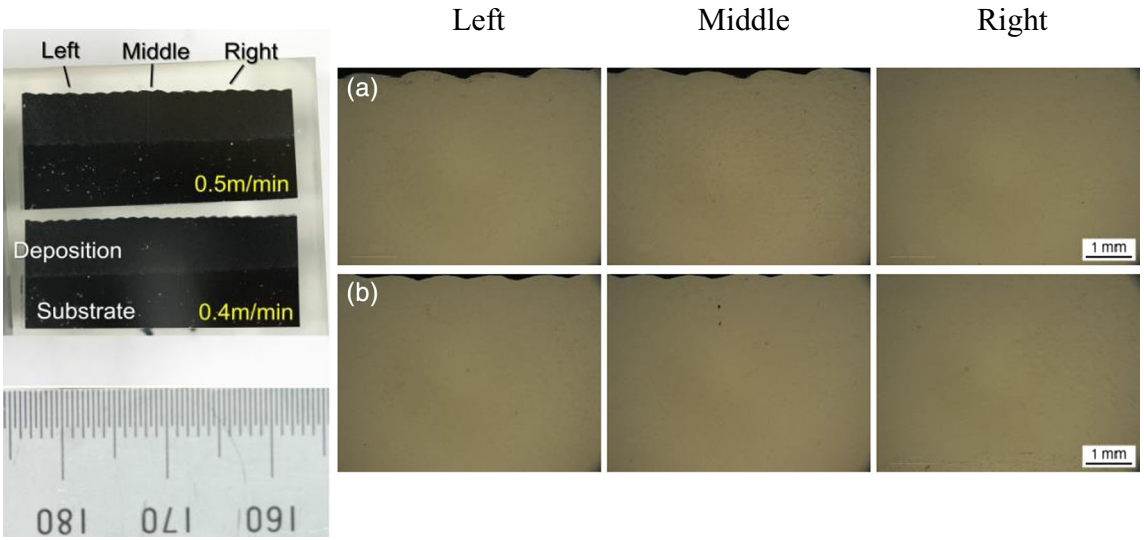

Fig. 7 Optical micrographs showing single layer deposit porosity with CMT-PADV process: **a** TS=0.5 m/min, HI=135.4 J/mm and **b** TS=0.4 m/min, HI=169.3 J/mm

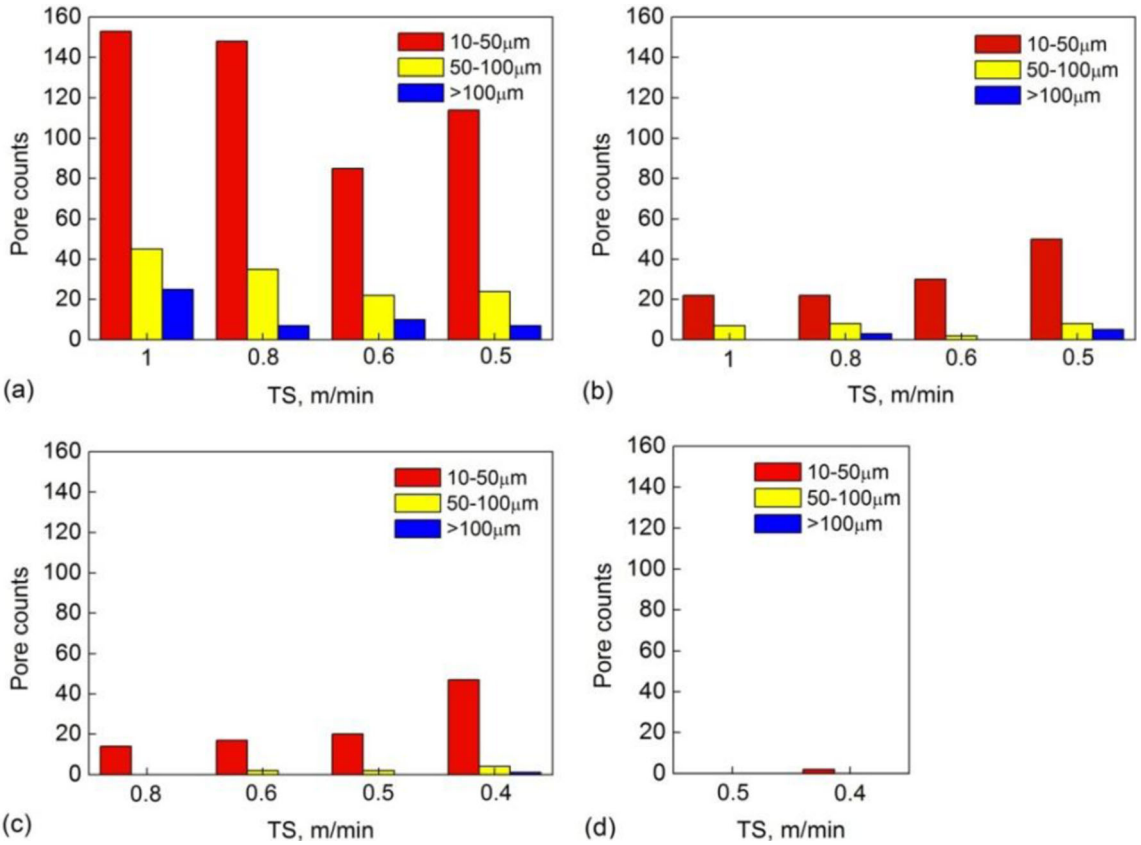

Fig. 8 Pore counts of single layer deposit samples using different modes: **a** CMT, **b** CMT-P, **c** CMT-ADV and **d** CMT-PADV (a 15-mm representative section of the entire single layer deposit 100 mm in length)

The detailed porosity generation mechanism of the single layer deposits produced by these different arc modes is further revealed by analysing the deposit geometry, microstructure and arc characteristics, respectively.

All the transverse profiles and the correlations between the geometry and TS are shown in Figs. 9 and 10, respectively. Compared to the CMT-P process a narrow finger-shaped molten pool developed during the conventional CMT process (Fig. 9a), which meant that although the deposit width (*B*) was similar and the melting depth (*H*) was higher than that of CMT-P (Fig. 10a, b), the total melted area of deposit (*MA*) was lower than that of CMT-P (Fig. 10c). Finger-shaped penetration with a lower melting depth and area was observed using the CMT-ADV process, as shown in Fig. 9c. The ratio $B/(DH+H)$ (where, *DH* means height of deposit) which indicates the aspect ratio of single layer bead was also calculated and is shown in Fig. 10d. With the same TS, the ratio using the CMT-P process was increased by about 10 % compared to that of the conventional CMT process. In comparison, the CMT-PADV process was quite different in that a spherical-shaped deposit was achieved with very low dilution (*H* was about 0.4 mm with different TS), as shown in Fig. 9d.

Figures 11, 12, 13 and 14 illustrate the microstructure of longitudinal sections of single layer deposits using the four different modes. During the conventional CMT and CMT-P process, a coarse columnar grain structure was observed as shown in Figs. 11 and 12, respectively. A mixture of finer columnar and equiaxed grain structure was observed using the CMT-ADV process (Fig. 13). Compared with the other three processes, the finest equiaxed grain structure was obtained using the CMT-PADV process. It can be explained that the grain size and morphology are predominantly affected by the HI level, and a lower HI can effectively refine the grain structure [14]. In addition, due to the lower HI in the CMT-ADV and CMT-PADV process, some phase particles which exist in the filler wire, such as Al_3Ti and Al_3Zr, can be preserved thus used as high efficiency heterogeneous nucleation particles to promote the formation of finer grain structure [15–17].

Porosity formation in aluminium alloy is mainly due to the mutation of hydrogen solubility in the process of liquid to solid state transformation. According to prior studies [18–20], cellular dendrite, dendritic solidification interface and some inclusions can be used as heterogeneous nucleation particles and there is a competition correlation

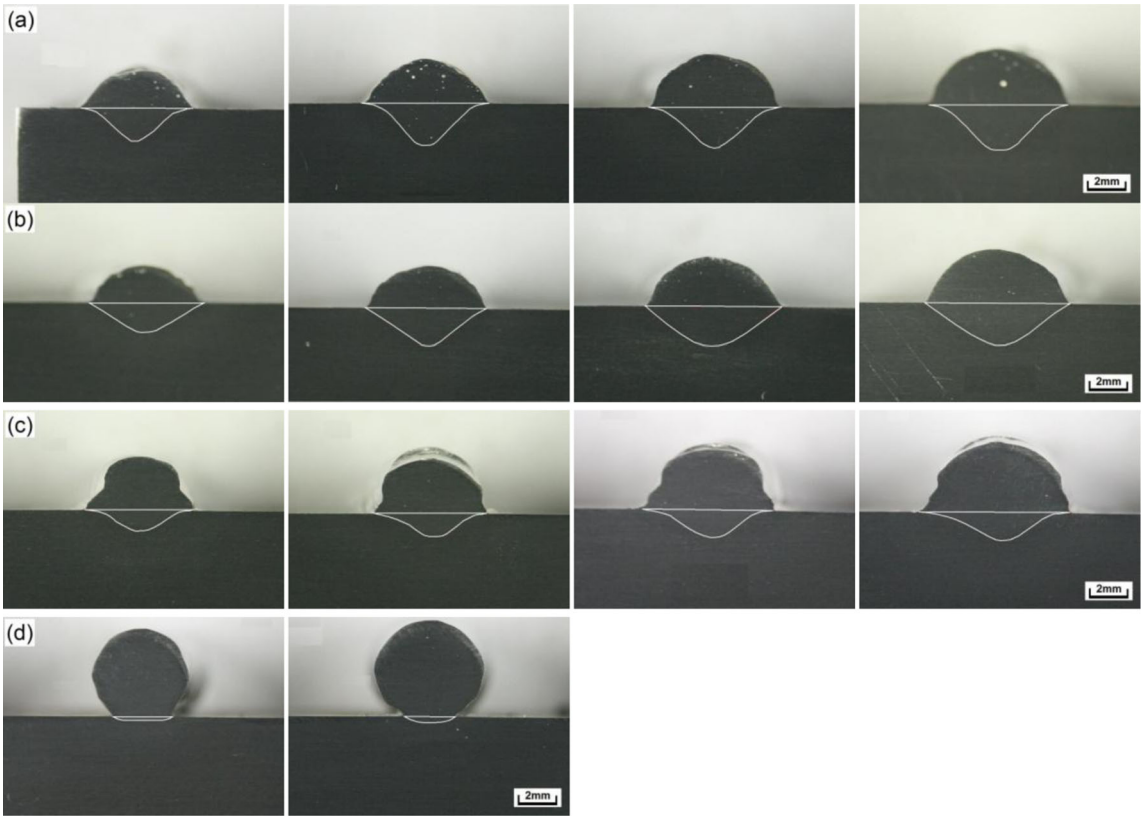

Fig. 9 Transverse section of single layer deposit samples using different modes: **a** CMT, TS=1.0–0.5 m/min, HI=165.8–331.6 J/mm, **b** CMT-P, TS=1.0–0.5 m/min, HI=183.4–366.8 J/mm, **c** CMT-ADV, TS=0.8–0.4 m/min, HI=170.8–341.6 J/mm and **d** CMT-PADV, TS=0.5–0.4 m/min, HI=135.4–169.3 J/mm (corresponding to TS decreasing from *left* to *right*)

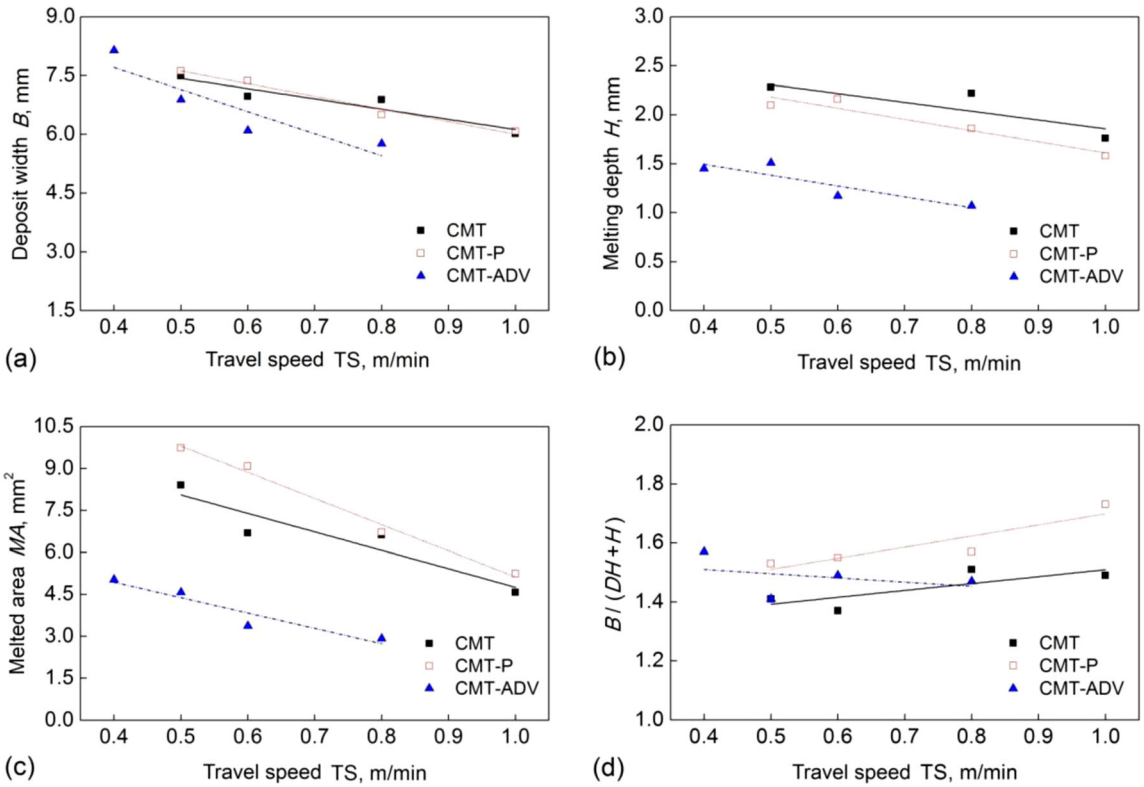

Fig. 10 Correlation between: **a** *B* and TS, **b** *H* and TS, **c** *MA* and TS and **d** *B*/(*DH*+*H*) and TS

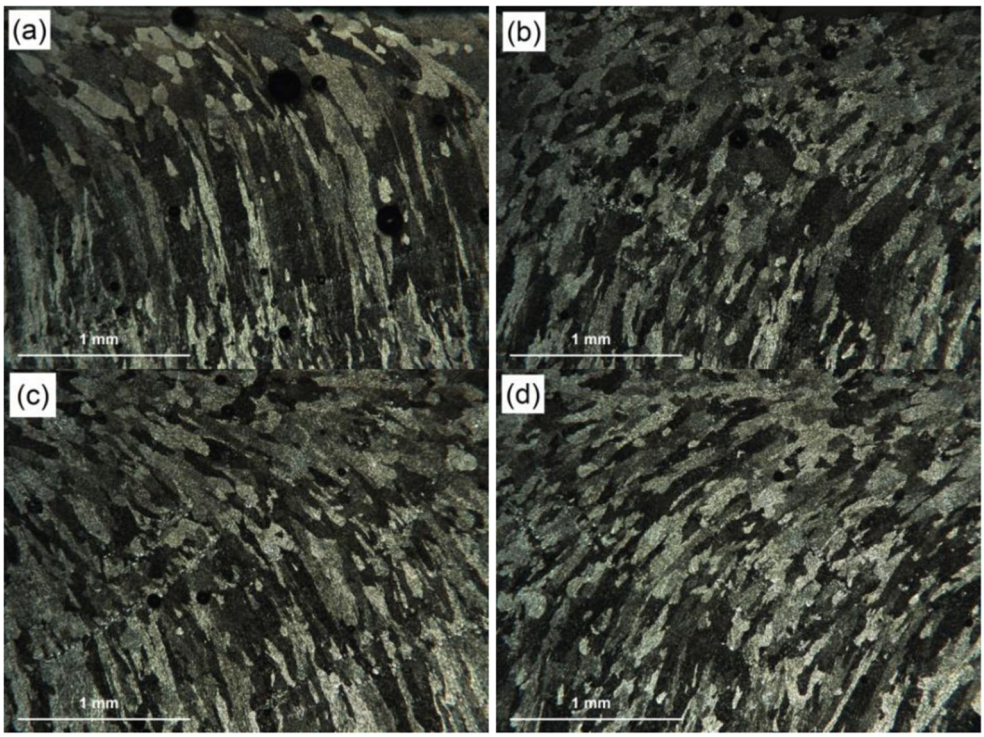

Fig. 11 Microstructure of single layer deposit samples using conventional CMT process: **a** TS=1.0 m/min, HI=165.8 J/mm, **b** TS=0.8 m/min, HI=207.3 J/mm, **c** TS=0.6 m/min, HI=276.3 J/mm and **d** TS=0.5 m/min, HI=331.6 J/mm

between dendrite growth and pore nucleation rate, so the porosity has a close relationship with the grain size [21]. During the conventional CMT process, a narrow finger-shaped molten pool developed which prevented the escape of gas pores [22, 23], in addition a coarse columnar grain structure developed, which also increased the porosity formation [24, 25]. Thus, a large number of pores were observed in the samples made with the conventional CMT process. During solidification, small pores float up and can combine into larger ones. These pores can also increase in

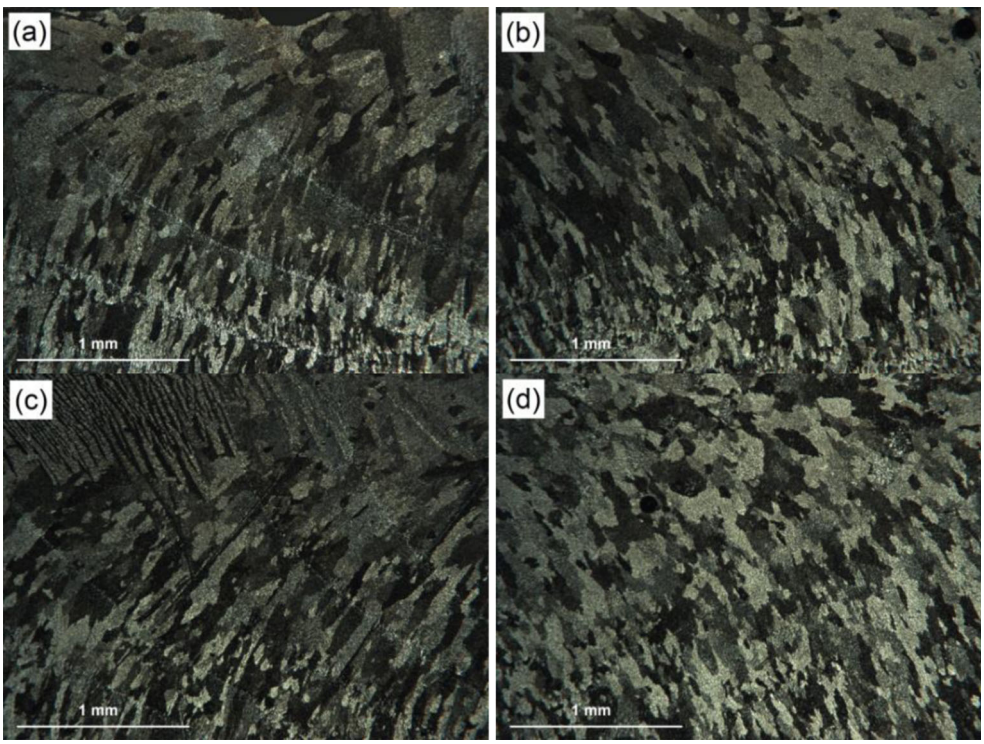

Fig. 12 Microstructure of single layer deposit samples using CMT-P process: **a** TS=1.0 m/min, HI=183.4 J/mm, **b** TS=0.8 m/min, HI=229.3 J/mm, **c** TS=0.6 m/min HI=305.7 J/mm and **d** TS=0.5 m/min, HI=366.8 J/mm

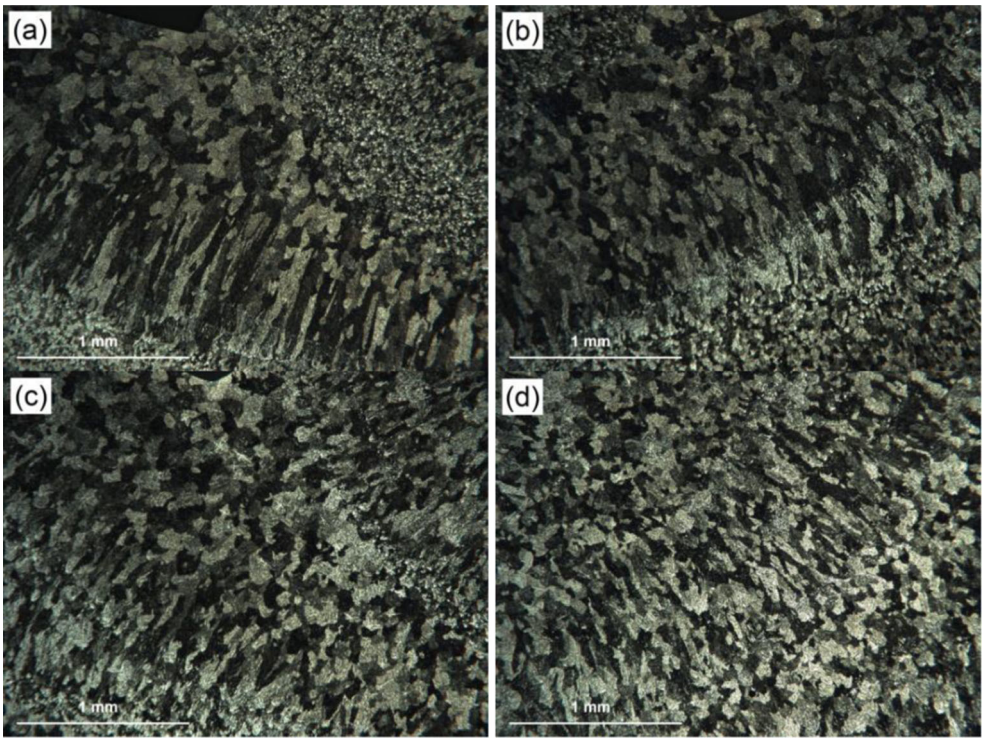

Fig. 13 Microstructure of single layer deposit samples using CMT-ADV process: **a** TS=0.8 m/min, HI=170.8 J/mm, **b** TS=0.6 m/min, HI=227.8 J/mm, **c** TS=0.5 m/min, HI=273.4 J/mm and **d** TS=0.4 m/min, HI=341.6 J/mm

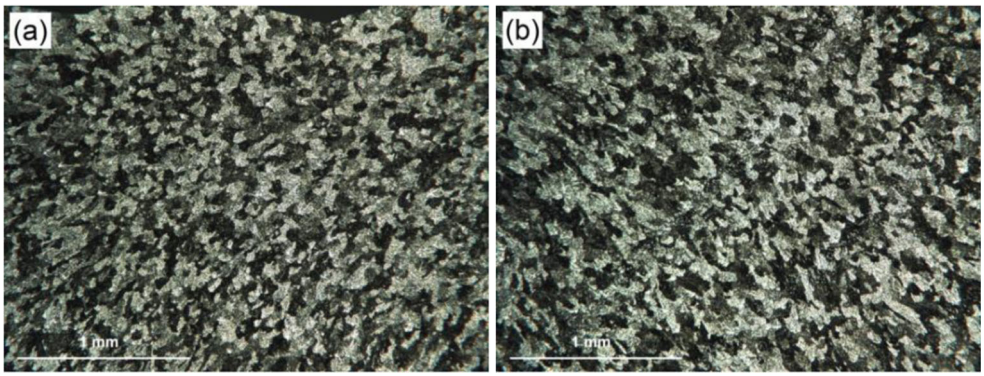

Fig. 14 Microstructure of single layer deposit samples using CMT-PADV process: **a** TS=0.5 m/min, HI=135.4 J/mm and **b** TS=0.4 m/min, HI=169.3 J/mm

size due to decreased pressure resulting in the large gas pores that were observed at the top part of the deposit.

Although the HI of the CMT-P process with the same TS was greater than that of the conventional CMT process, the porosity was still significantly reduced. It can be explained that the area of molten pool was increased and the ratio of $B/(DH+H)$ was higher. This means that the escape distance is of gas pores is decreased, and therefore, the likelihood of escape is increased. In addition, the fluidity of liquid metal in the molten pool was enhanced due to the effect of pulsed current [22, 26–28] which provided more opportunity for gas pore escape.

In the CMT-ADV process, a finger-shaped penetration with lower H and the mixture of finer columnar and

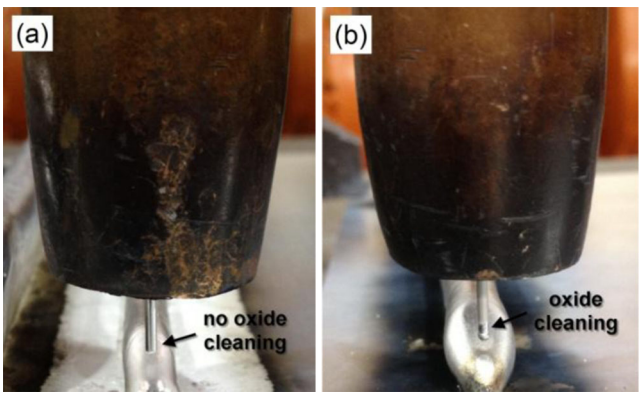

Fig. 15 Ends of Al-6.3%Cu wire using different modes: **a** CMT-P and **b** CMT-ADV

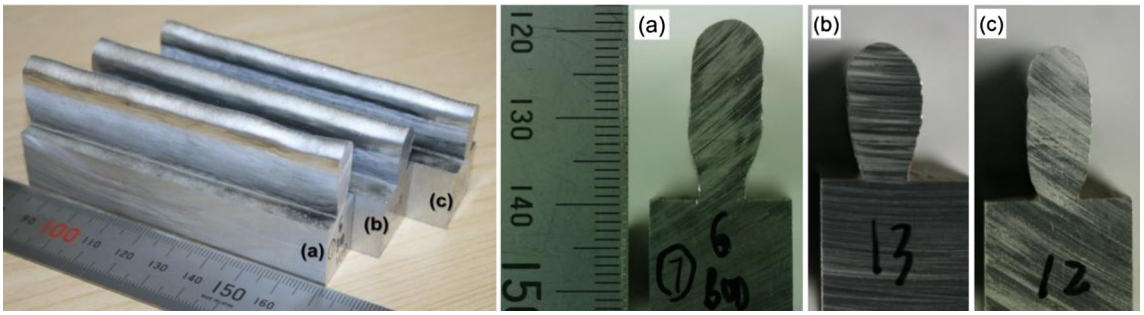

Fig. 16 Profile and transverse sections of additively manufactured wall samples using CMT-P process: **a** WFS=6 m/min, TS=1.0 m/min, 20 layers, 20.5 mm in height, **b** WFS=6 m/min, TS=0.8 m/min, 14 layers, 16 mm in height and **c** WFS=5 m/min, TS=0.8 m/min, 14 layers, 17 mm in height

equiaxed grain structure was observed. Although the finger-shaped penetration is not beneficial in terms of gas pore escape, much shallower penetration was generated by the CMT-ADV process which significantly reduced its influence on the gas pore escape. Compared with the CMT-P process, the grain structure was further refined due to a lower HI of CMT-ADV process. In addition due to the alternating polarities of the arc the CMT-ADV process can produce a significant oxide cleaning effect on the end of the Al-6.3 % Cu wire [29] (Fig. 15). This reduces the hydrogen content which is contained in the oxidation layer, entering into the molten pool. In addition, the AC arc can also cause the stirring of molten pool with the polarity change in every cycle [30] which is beneficial in the gas pore escape. The CMT-PADV process was observed to have low dilution and a fine equiaxed grain structure. This process combines the advantages of the CMT-P and CMT-ADV processes which makes it the most efficient process in terms of reducing and even eliminating the porosity. In addition, the chance of getting hydrogen from the substrate is also reduced due to its low dilution.

It can be summarised from the above analysis that the conventional CMT process generates the highest level of porosity due to its high HI, the narrow finger-shaped molten pool and the coarse grain structure. This process

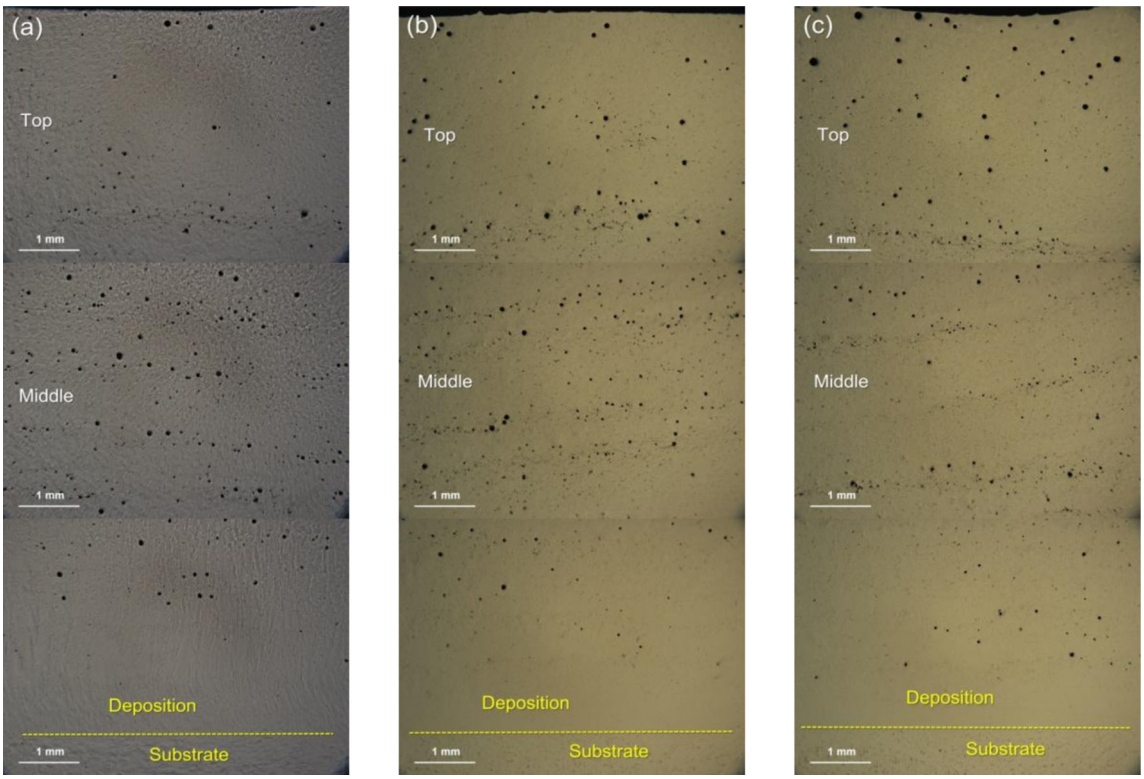

Fig. 17 Longitudinal porosity of additively manufactured wall samples using CMT-P process: **a** WFS=6 m/min, TS=1.0 m/min, HI=151.3 J/mm, **b** WFS=6 m/min, TS=0.8 m/min, HI=189.1 J/mm and **c** WFS=5 m/min, TS=0.8 m/min, HI=137.1 J/mm

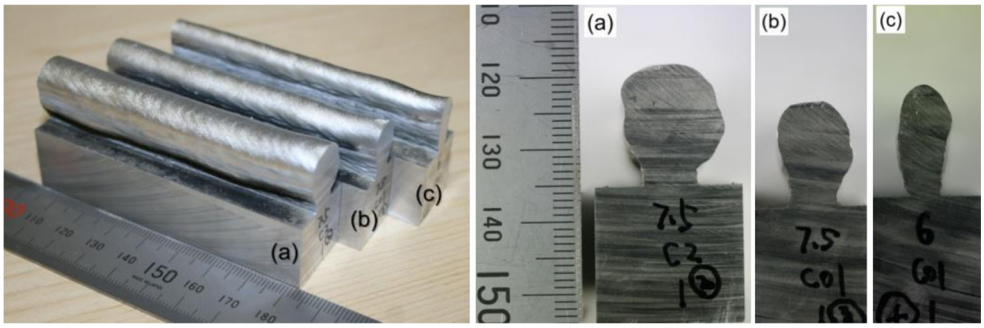

Fig. 18 Profile and transverse sections of additively manufactured wall samples using CMT-ADV process: **a** WFS=7.5 m/min, TS=0.5 m/min, 10 layers, 17 mm in height, **b** WFS=7.5 m/min, TS=0.8 m/min, 10 layers, 14 mm in height and **c** WFS=6 m/min, TS=0.8 m/min, 10 layers, 15 mm in height

is considered not suitable for the WAAM process. The other three processes can significantly reduce the porosity of single layer deposit. In the next section, the porosity of multilayer deposition using CMT-P, CMT-ADV and CMT-PADV process are analysed.

3.2 Multilayer deposition using CMT-P process

The multilayer additively manufactured Al-6.3%Cu wall samples were produced with different WFS and TS using the CMT-P process. The profiles and transverse sections are shown in Fig. 16. It can be seen that the surface of each sample is smooth and uniform. The average layer height is about 1 mm for each sample. Figure 17 shows the porosity distribution in a longitudinal section of 5 mm for these three samples. It is observed that even with different HI (137.1–189.1 J/mm), the porosity of the three samples is similar. A very few small pores were generated in the first three layers. Larger pores around 50 μm in diameter were generated near the top of the wall. The gas pores were observed with a strip distribution centred on the layer boundaries.

As described in Section 3.1, a number of micro-pores with a diameter of less than 20 μm were distributed in the

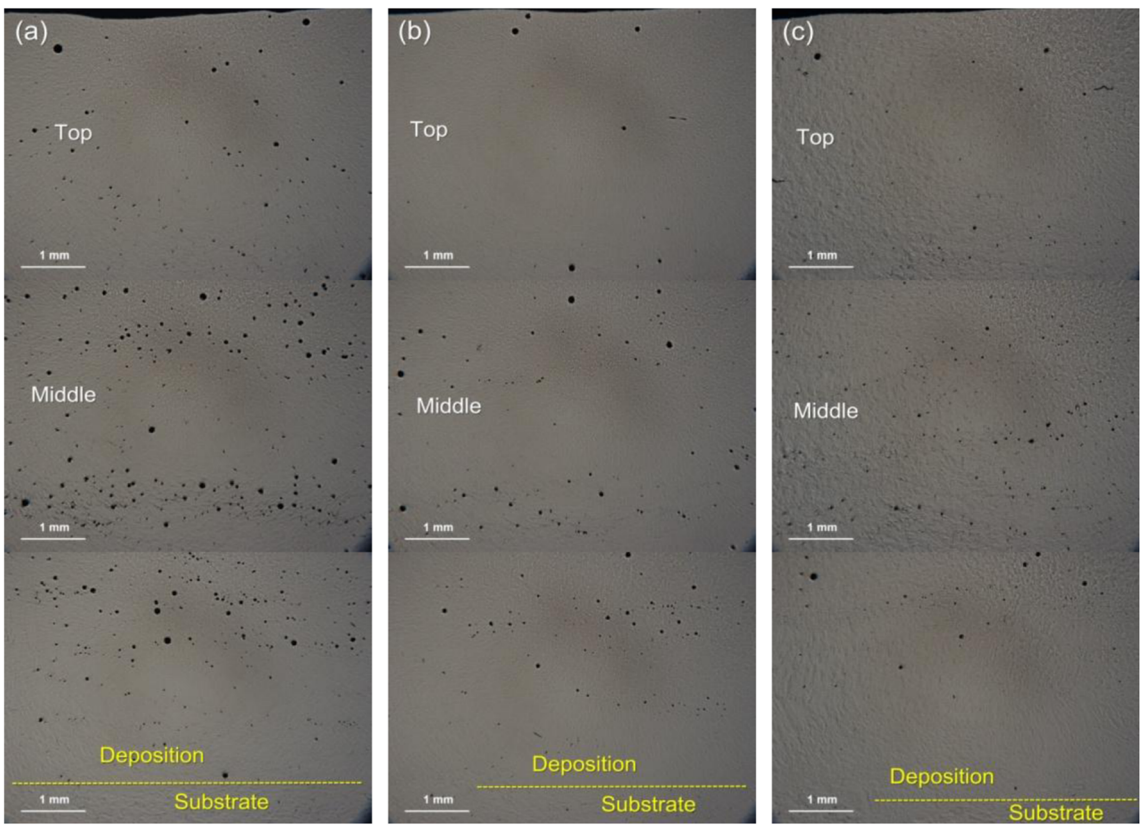

Fig. 19 Longitudinal porosity of additively manufactured samples using CMT-ADV process: **a** WFS=7.5 m/min, TS=0.5 m/min, HI=273.4 J/mm, **b** WFS=7.5 m/min, TS=0.8 m/min, HI=170.8 J/mm and **c** WFS=6 m/min, TS=0.8 m/min, HI=135.7 J/mm

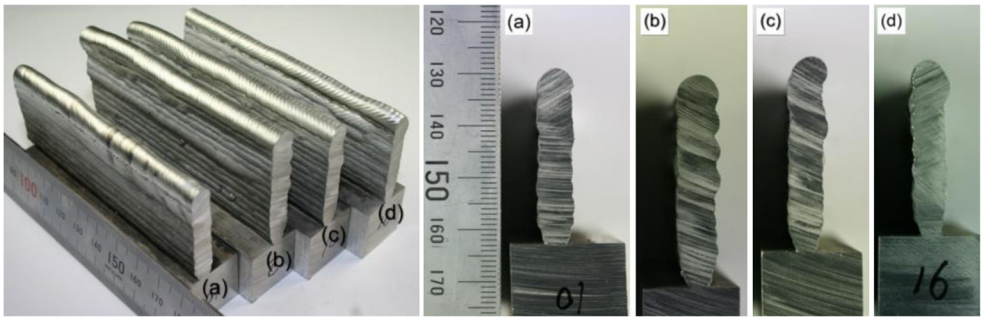

Fig. 20 Profile and transverse sections of additively manufactured wall samples using CMT-PADV process: **a** WFS=7.5 m/min, TS=0.5 m/min, 10 layers, 33.6 mm in height, **b** WFS=6 m/min, TS=0.4 m/min, 14 layers, 41 mm in height, **c** WFS=6 m/min, TS=0.5 m/min, 14 layers, 41.4 mm in height and **d** WFS=6 m/min, TS=0.6 m/min, 14 layers, 33.5 mm in height

upper part of single layer deposit (Fig. 8b). When the previous layer is re-melted by the new layer, these micro-pores can be used as efficient heterogeneous nucleation particles to form new pores during the solidification. These newly formed pores are trapped and exist in the layer boundary.

3.3 Multilayer deposition using CMT-ADV process

Multilayer additively manufactured wall samples were produced with different WFS and TS using the CMT-ADV process. It was observed that the wall profile and porosity are influenced predominantly by HI (135.7–273.4 J/mm), as shown in Figs. 18 and 19, respectively. In general, the wall geometry is irregular and gas pores cannot be suppressed. The wall profile improves and the gas pores were reduced with a decrease of HI.

From the single layer deposit using CMT-ADV process, a fish-scale pattern can be seen (as shown in Fig. 6). The height difference between the crest and trough was more than 0.5 mm and the distance between the adjacent crests varied from 2.4 to 5.2 mm with TS varying from 0.4 to 1.0 m/min. Because of this rough profile, droplet transformation was not stable during the multilayer AM process, which resulted in poor wall geometry. In addition,

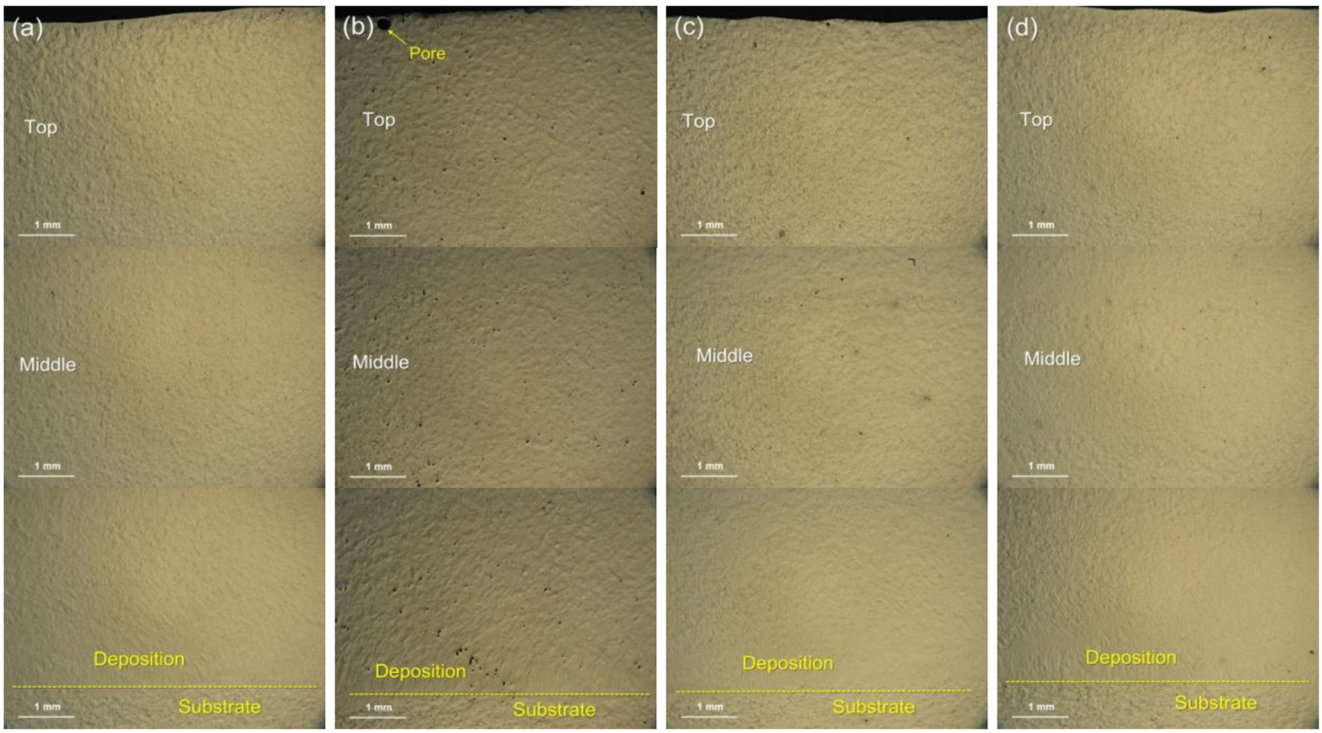

Fig. 21 Longitudinal porosity of additively manufactured wall samples using CMT-PADV process: **a** WFS=7.5 m/min, TS=0.5 m/min, HI=154.7 J/mm, **b** WFS=6 m/min, TS=0.4 m/min, HI=168.4 J/mm, **c** WFS=6 m/min, TS=0.5 m/min, HI=134.7 J/mm and **d** WFS=6 m/min, TS=0.6 m/min, HI=112.2 J/mm

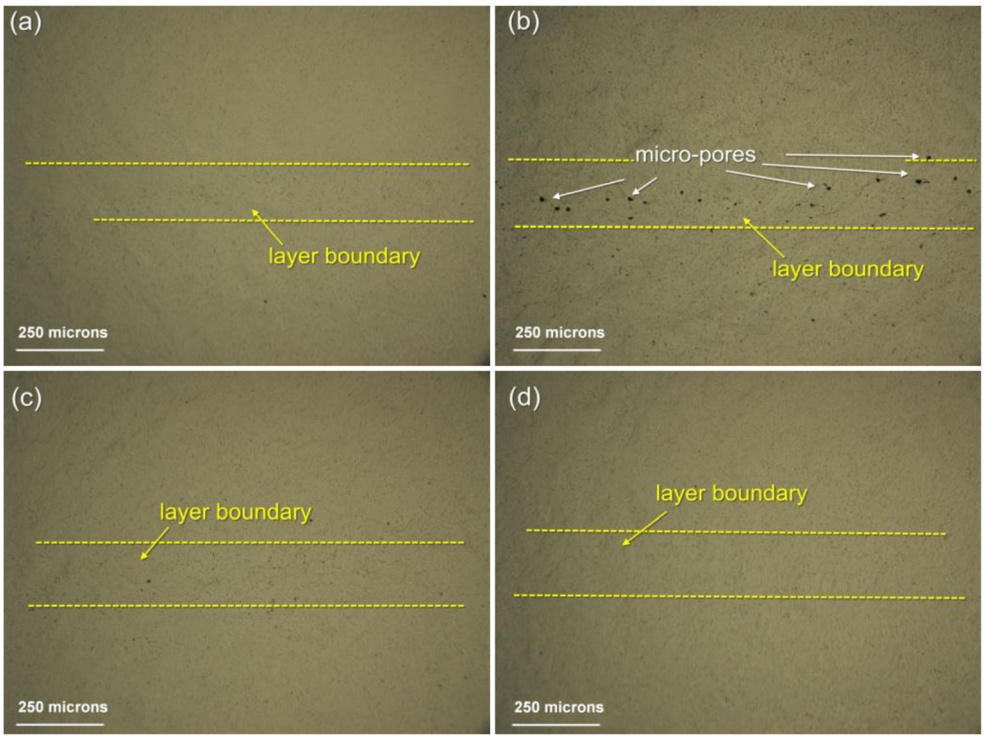

Fig. 22 Upper part layer boundary of additively manufactured wall samples using CMT-PADV process: **a** WFS=7.5 m/min, TS=0.5 m/min, HI=154.7 J/mm, **b** WFS=6 m/min, TS=0.4 m/min, HI=168.4 J/mm, **c** WFS=6 m/min, TS=0.5 m/min, HI=134.7 J/mm and **d** WFS=6 m/min, TS=0.6 m/min, HI=112.2 J/mm

oxidation in the troughs of the deposition cannot be effectively cleaned and this can act as efficient heterogeneous nucleation particles to promote pore formation.

3.4 Multilayer deposition using CMT-PADV process

The multilayer additively manufactured wall samples were produced with different WFS and TS using the CMT-PADV process. The profile and transverse sections are shown in Fig. 20. It can be seen that the wall configuration was significantly influenced by HI (112.2–168.4 J/mm). A better wall profile was obtained with a HI of 154.7 J/mm. The wall profile was worse when HI was higher (Fig. 20b, 168.4 J/mm) or lower (Fig. 20c, d; 134.7 and 112.2 J/mm).

Figure 21 shows the porosity in a longitudinal section of these four wall samples. It can be observed that there is almost no porosity, except for the sample with high HI (Fig. 21b). Figure 22 shows the upper part of the samples with a larger magnification. A certain number of micro-pores with the diameter of about 10–15 μm were distributed around the layer boundary produced with the highest HI of 168.4 J/mm. This can be explained in that the re-melted solidification structure is coarser in the layer boundary (Fig. 23), and the dendritic solidification interface can be used as efficient nucleation particles for gas pores. The deposit dilution is enhanced with the increase of HI, which can promote the nucleation and growth of gas pores.

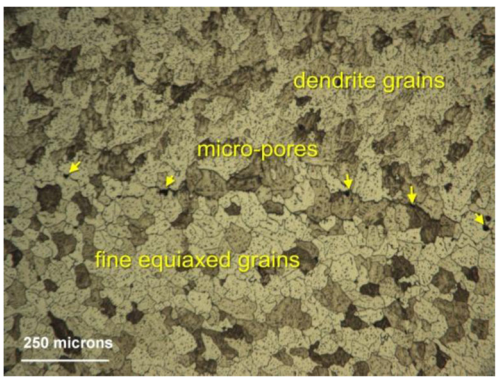

Fig. 23 Upper part layer boundary microstructure of additively manufactured wall sample: (b in Fig. 22) WFS=6 m/min, TS=0.4 m/min, HI=168.4 J/mm

4 Conclusions

The porosity characteristic of Al-6.3%Cu alloy during the WAAM process was systematically investigated in this study. It was observed that the deposit porosity can be significantly influenced by different arc modes in the CMT process. Among all the four arc modes, CMT-PADV is the most suitable process for the WAAM process of this aluminium alloy. With proper control of the heat input this process may produce walls with no porosity. The effect of porosity elimination using the CMT-PADV process can be reasonably

explained by its low heat input, fine equiaxed grains and effective oxide cleaning of the wire.

Acknowledgments The authors would like to thank all the WAAMat Programme members for their support.

References

1. Ding J, Colegrove P, Mehnen J, Ganguly S, Sequeira Almeida PM, Wang F, Williams S (2011) Thermo-mechanical analysis of wire and Arc additive layer manufacturing process on large multi-layer parts. Comp Mater Sci 50:3315–3322
2. Wang F, Williams S, Colegrove P, Antonysamy AA (2013) Microstructure and mechanical properties of wire and arc additive manufactured Ti-6Al-4 V. Metall Mater Trans A 44A:968–977
3. Wang HJ, Jiang WH, Ouyang JH, Kovacevic R (2004) Rapid prototyping of 4043 Al-alloy parts by VP-GTAW. J Mater Process Technol 148:93–102
4. Ouyang JH, Wang HJ, Kovacevic R (2002) Rapid prototyping of 5356-aluminum alloy based on variable polarity gas tungsten arc welding: process control and microstructure. Mater Manuf Process 17:103–124
5. Liu WL (2007) Rapid prototyping technology of Al-alloy parts by AC-TIG. Tianjin University, Tianjin
6. Buchbinder D, Schleifenbaum HB, Heidrich SB, Meiners WB, Bültmann J (2011) High power selective laser melting (HP SLM) of aluminum parts. Phys Procedia 12:271–278
7. Brandl E, Heckenberger U, Holzinger V, Buchbinder D (2012) Additive manufactured AlSi10Mg samples using selective laser melting (SLM): microstructure, high cycle fatigue, and fracture behavior. Mater Des 34:159–169
8. Feng JC, Zhang HT, He P (2009) The CMT short-circuiting mental transfer process and its use in thin aluminum sheets welding. Mater Des 30:1850–1852
9. Pickin CG, Young K (2006) Evaluation of cold metal transfer (CMT) process for welding aluminum alloy. Sci Technol Weld Joi 11:583–585
10. Pickin CG, Williams SW, Lunt M (2011) Characterization of the cold metal transfer (CMT) process and its application for low dilution cladding. J Mater Process Technol 211:496–502
11. Cook GE, Eassa EH (1985) The effect of high-frequency pulsing of a welding arc. IEEE Trans Indust Appl 1A–21:1294–1299
12. Pépe N, Egerland S, Colegrove P, Yapp D, Leonhartsberger A, Scotti A (2011) Measuring the process efficiency of controlled gas metal arc welding processes. Sci Technol Weld Joi 16:412–417
13. Dupont JN, Marder AR (1995) Thermal efficiency of arc welding processes. Weld J 12:406s–416s
14. Kamal P, Surjya KP (2011) Effect of pulse parameters on weld quality in pulsed gas metal arc welding: a review. J Mater Eng Perf 20:918–931
15. Kou S, Le Y (1986) Nucleation mechanisms and grain refining of weld metal. Weld J 65:305s–313s
16. Yunjia H, Frost RH, Olson DL, Edwards GR (1989) Grain refinement of aluminum weld metal. Weld J 68:280s–289s
17. Guo XM, Yang CG, Qian BN, Xu Q, Zhang HY (2005) Effects of inoculants Ti and Zr on the microstructures and properties of 2219 Al-Cu alloy welds. Acta Metall Sin 41: 397–401
18. Xing JD (1993) Formation and prevention of gas pore in aluminum alloy. Spe Cast Nonfer Alloy 14:30–34
19. Shu D, Sun BD, Wang J (1998) Nucleation mechanism of gas pore in aluminum alloy. Found Eng 22:49–52
20. Xu LH, Tian ZL, Zhang XM, Peng Y (2006) Effects of shielding gas on microstructure and number of gas pore in high strength aluminum alloys weld. Trans Chn Weld Inst 27:69–72
21. Li KD, Chang E (2004) Mechanism of nucleation and growth of hydrogen porosity in solidifying A356 aluminum alloy: an analytical solution. Acta Mater 52:219–231
22. Kou S, Wang YH (1986) Weld pool convection and its effect. Weld J 3:63s–70s
23. Devletian JH, Wood WE (1983) Factors affecting porosity in aluminium welds—a review. WRC Bull 290:1–18
24. Li ZY, Zhu MF, Dai T (2013) Modeling of microporosity formation in an Al-7%Si alloy. Acta Metall Sin 49:1032–1040
25. Lee PD, Hunt JD (2001) Hydrogen porosity in directionally solidified aluminium-copper alloys: a mathematical model. Acta Mater 49: 1383–1398
26. Sun JS, Wu CS (2002) The influence of heat input on the MIG weld pool behaviour. Sci Chn E 32:465–471
27. Lin ML, Eagar TW (1985) Influence of arc pressure on weld pool geometry. Weld J 64:162s–169s
28. Silva CLM, Scotti A (2006) The influence of double pulse on porosity formation in aluminium GMAW. J Mater Process Technol 171:366–372
29. Harwig DD, Dierksheide JE, Yapp D, Blackman S (2006) Arc behavior and melting rate in the VP-GMAW process. Weld J 3: 52s–62s
30. Kumar R, Dilthey U, Dwivedi DK, Ghosh PK (2009) Thin sheet welding of Al 6082 alloy by AC pulse-GMA and AC wave pulse-GMA welding. Mater Des 30:306–313